

1                   **Decadal-scale morphological adjustment of a lowland tropical river**

2           Elizabeth H. Dingle<sup>a,b\*</sup>, Enrico C. Paringit<sup>c</sup>, Pamela L.M. Tolentino<sup>d</sup>, Richard D. Williams<sup>a</sup>,  
3                   Trevor B. Hoey<sup>a</sup>, Brian Barrett<sup>a</sup>, Hazel Long<sup>a</sup>, Crystal Smiley<sup>a</sup>, Eilidh Stott<sup>a</sup>

4  
5   <sup>a</sup>. School of Geographical and Earth Sciences, University of Glasgow, United Kingdom

6   <sup>b</sup>. Department of Geography, Faculty of Environment, Simon Fraser University, Canada

7   <sup>c</sup>. Geodetic Engineering, University of Philippines – Diliman, Philippines

8   <sup>d</sup>. National Institute of Geological Sciences, University of Philippines – Diliman, Philippines

9

10   \* Corresponding author. E-mail address: [elizabeth\\_dingle@sfu.ca](mailto:elizabeth_dingle@sfu.ca) (Elizabeth H. Dingle)

11

12   **Abstract**

13

14   Compared with temperate regions, much less is known about the dynamics of tropical river  
15   systems. Tropical rivers are typically characterised by pronounced seasonal changes in  
16   precipitation, large sediment loads and high rates of lateral channel migration across often  
17   very low-gradient and densely populated floodplains. Understanding the controls on channel  
18   migration or change is integral to our ability to fully predict and build resilience against flood  
19   risk and wider river-related hazards. Here, we analyse channel and confluence migration over  
20   the last ~40 years along a ~85 km reach of the Cagayan River and one of its tributaries, the  
21   Pinacanauan de Ilagan (Luzon, Philippines) using optical satellite imagery captured during  
22   this period. Combining this with spatial variations in channel pattern, valley width and new bed  
23   material grain size data, we demonstrate that sediment transport and deposition are key  
24   drivers of the observed tropical channel morphodynamics in this region. The high sediment  
25   supply generated in the catchment headwaters (by mass-wasting of hillslopes triggered  
26   especially in typhoons) results in high aggradation rates and channel widening on the lower  
27   gradient alluvial plain. We suggest that this aggradation enhances local confluence and lateral  
28   channel migration rates, which can reach more than 300 m per decade, and that lateral

29 migration rates of tropical rivers are typically greater than those of temperate rivers. Channel  
30 morphodynamics have implications for how to best manage these types of tropical river  
31 systems, where hard bank protection structures may result in a complex geomorphic response  
32 and flood risk mapping may need to include assessment of sensitivity to varying channel  
33 position and topography.

34

35 Keywords: tropical rivers, channel migration, sediment dynamics, flood risk, Philippines

36

## 37 1. Introduction

38

39 Tropical river systems are often characterised by highly seasonally variable water discharges,  
40 large sediment loads (e.g., Milliman and Meade, 1983; Gran et al., 2011; Syvitski et al., 2014)  
41 and rapid lateral channel migration rates (e.g., meander migration, avulsion, chute cut-off)  
42 across low-gradient and, in many instances, densely populated alluvial floodplains (Ashworth  
43 and Lewin, 2012; Darby et al., 2013; Constantine et al., 2014; Dixon et al., 2018; Suizu and  
44 Nanson, 2018). As channels migrate, they erode large parts of their floodplain which can result  
45 in the loss of property, infrastructure and productive farmland. These mobile channels also  
46 control patterns of sediment storage and release across the catchment, which influence  
47 downstream sediment budgets and pollutant transfer pathways (e.g., mine tailings) (Aalto et  
48 al., 2008). Understanding the controls on channel migration or change is integral to our ability  
49 to fully predict and build resilience to both flood risk and wider river-related hazards across  
50 these dynamic landscapes. Such understanding is paramount in large Asian river systems,  
51 where the effects of climate change are predicted to have the greatest impact on future global  
52 flood risk (Tolentino et al., 2016; Alfieri et al., 2017) as a result of changing El Niño Southern  
53 Oscillation (ENSO) conditions and seasonal rainfall patterns.

54

55 Compared with temperate regions, less is known about the behaviour of tropical rivers, defined  
56 here as being those located within the tropical climate belt and so experiencing warm

57 temperatures with little intra-annual variability, and having significant seasonal changes in  
58 precipitation (e.g., Syvitski et al., 2014). Many tropical regions are also prone to extreme  
59 meteorological events (e.g., typhoons, tropical cyclones), driving short-lived and highly  
60 elevated water and sediment discharges. It has been shown that: (i) tropical river channel  
61 patterns are not well-represented in global databases; (ii) the controls over sediment transport  
62 and channel change may differ from more temperate regions due to differences in hydrology  
63 (strong seasonality, typhoon event frequency and magnitude) and catchment properties (soil  
64 type, land use and disturbance); and, (iii) channel response to environmental disturbance is  
65 significant in the cases where it has been quantified (e.g., Latrubesse et al., 2005; Syvitski et  
66 al., 2014; Dewan et al., 2017; Horton et al., 2017). Whether controls on tropical river  
67 morphology and dynamics are fundamentally different from those in more temperate settings  
68 remains unresolved within the literature (Latrubesse et al., 2005; Scatena and Gupta, 2013;  
69 Syvitski et al., 2014; Plink-Björklund, 2015). More recently, changes in tropical forest cover  
70 has also been demonstrated to enhance lateral rates of channel mobility through a reduction  
71 in bank shear strength and changes in pore water pressure (and therefore bank sediment  
72 cohesion) as a result of reduced rainfall interception by forest canopy cover (Horton et al.,  
73 2017). Deforestation in the Kinabatangan River (Malaysia) has been suggested as the  
74 principal driver of enhanced lateral channel migration rates, by over 20%, in comparison to  
75 forested regions over the same 25-year period (Horton et al., 2017). However, the effects of  
76 deforestation and land use change on lateral channel migration rates have only been tested  
77 in a limited number of tropical systems to date. While enhanced migration rates through  
78 changes in land use in tropical environments have been previously documented (e.g., Horton  
79 et al., 2017), these trends are not consistent in all tropical environments. The Aguapeí River  
80 in Brazil was largely deforested by 1962, yet channel migration rates were found to decrease  
81 between 1962-2010 (Suizu and Nanson, 2018). This was attributed to an ENSO-driven  
82 increase in peak flow discharge resulting in channel widening and a reduction in channel  
83 sinuosity.

84

85 This paper presents and analyses new data on channel and confluence migration, channel  
86 pattern, width and sediment grain size from a tropical river system. The analysis tests the  
87 hypothesis that tropical rivers have higher migration rates than comparable temperate  
88 systems (e.g., similar catchment area, gradient, annual mean flow), and that these migration  
89 rates may be independent of land use change. We examine a range of factors (e.g., climate  
90 and hydrology) that may result in tropical rivers having different morphological characteristics.  
91 We first test whether boundary conditions in tropical river systems, which differ from those in  
92 temperate rivers, drive high migration rates. The key boundary conditions in this landscape  
93 are rates of sediment supply from upstream and the magnitude and frequency of flood  
94 hydrographs, dominated by typhoons which generate several geomorphically effective flows  
95 each year. We quantify rates of lateral channel migration based on observations over the past  
96 ~40 years and then examine confluence migration patterns, channel pattern, width, valley  
97 confinement and downstream bed grain size variation and consider the impact of sediment  
98 dynamics on modern river morphology. Channel morphology and rates of change are  
99 compared with published data to allow evaluation of the hypothesis above. Finally, we explore  
100 whether lateral channel and confluence migration represents a significant hazard to  
101 communities living along tropical river banks and consider the implications for river and flood  
102 risk management.

103

104 Analysis was undertaken on the Cagayan River (27,700 km<sup>2</sup>) where it passes through Isabela  
105 province, in the eastern part of Luzon Island in the Philippines (Fig. 1). The extensive alluvial  
106 floodplain of the main Cagayan channel and a number of its tributaries make this an ideal  
107 setting to observe large scale patterns of sediment erosion, deposition and channel migration  
108 over a period of ~40 years (the period over which satellite imagery is available). The Cagayan  
109 River is the largest river system on Luzon and supplies fresh water and nutrient rich sediments  
110 to a catchment population of more than 3.45 million (2015 census data). Typically, the  
111 Philippines experiences multiple typhoons each year, although not all represent significant  
112 hazards. Typhoons of particular note in the last 15 years include Typhoons Haururot (known

113 internationally as typhoon Imbudo, 2003), Lando (Koppu, 2015) and Lawin (Haima, 2016),  
114 which resulted in more than \$300 million USD of damage across the Cagayan catchment  
115 (mainly to infrastructure and agricultural land), over 100 deaths and the displacement of more  
116 than 100,000 people nationwide (Floresca and Paringit, 2017). Typhoon Ompong (Mangkhut)  
117 in September 2018 caused significant damage and loss of life after the fieldwork reported in  
118 this paper. Despite this risk, populations living on the Cagayan River floodplain have  
119 continued to expand by 1-2% annually due to economic opportunities from tilling its fertile soils  
120 (Balderama et al., 2017). Deforestation across Luzon Island may have impacted sediment  
121 dynamics across parts of the Cagayan catchment. Analysis of maps (1934) and Landsat  
122 satellite imagery (captured in 2010) suggest a ~60% reduction in forest cover across the  
123 Philippines over this 76-year period (Forest Management Bureau, 2013). Under these  
124 conditions, an improved understanding of how sediment dynamics influence channel mobility  
125 is paramount in developing effective river management, hazard mitigation and land use  
126 strategies.

127

### 128 1.1. Regional geomorphological context

129

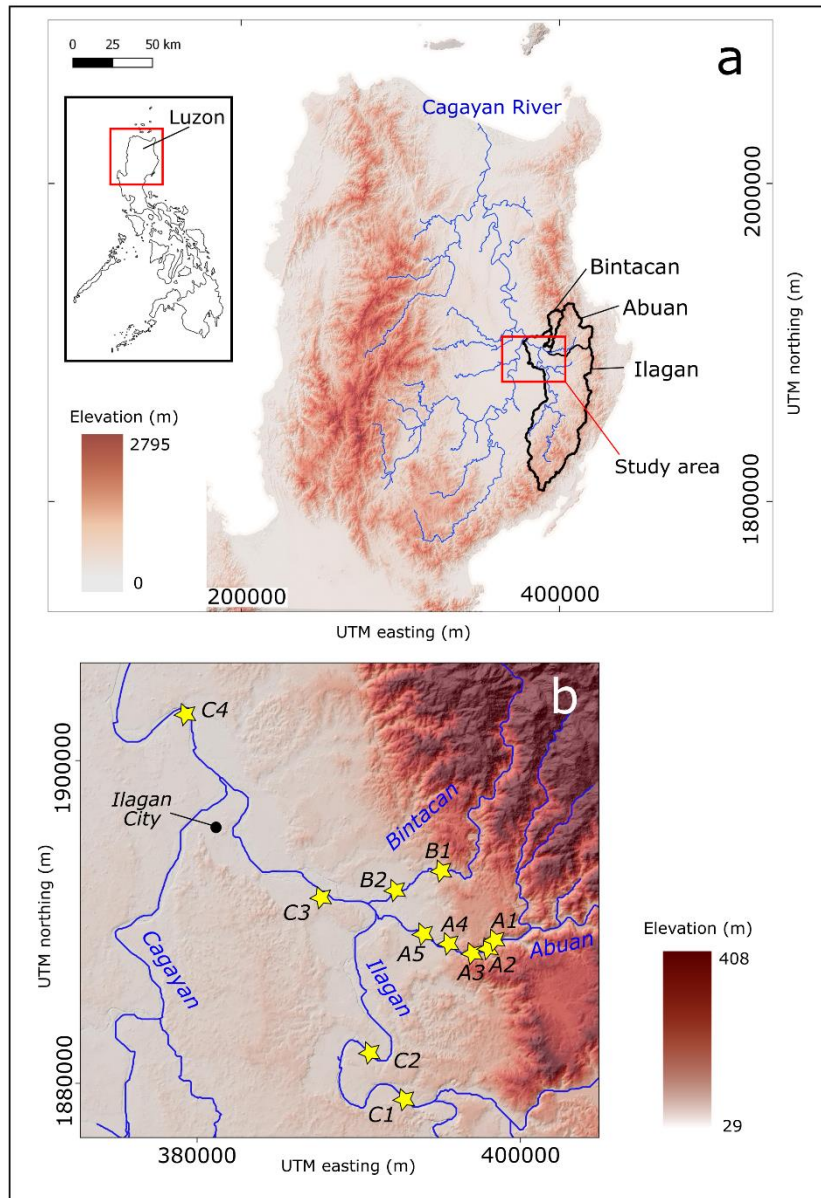
130 Luzon Island has a diverse tectonic, geologic, and climatic setting which generates spatial  
131 differences in the geomorphological characteristics, including topographic relief, channel  
132 gradient, drainage density and floodplain confinement of catchments and their river channels.  
133 These characteristics result from the nature and rates of processes through which sediment  
134 is eroded from the landscape (e.g., Tucker and Slingerland, 1997; Perron et al., 2008; Clubb  
135 et al., 2016) and drive variability in channel morphology (e.g., channel planform, lateral  
136 migration rate) and patterns of sediment storage and release as sediment is transported  
137 through the catchment (Lauer and Parker, 2008). The Cagayan River is the largest catchment  
138 on Luzon Island, covering an area of ~27,700 km<sup>2</sup> and is formed of four major tributaries (the  
139 Magat, Chico, Ilagan and Pinacanauan rivers), sourced in the surrounding Caraballo,  
140 Cordillera and Sierra Madre mountain ranges. The Pinacanauan de Ilagan River, catchment

141 area ~3,000 km<sup>2</sup>, drains the south east region of the Cagayan catchment. The Abuan (490  
142 km<sup>2</sup>) and Bintacan (111 km<sup>2</sup>) Rivers form the northeast portion of the Pinacanauan de Ilagan  
143 catchment (Fig. 1) and the headwaters of both are in the Sierra Madre mountain range, with  
144 a maximum elevation of 1,871 m (Mt. Cresta). The portion of the Pinacanauan de Ilagan  
145 catchment which does not include the Bintacan or Abuan catchments shall be referred to as  
146 the Ilagan catchment, as shown in Fig. 1a. The western portion of the Northern Sierra Madre  
147 mountain range, particularly in the province of Isabela, is characterised by Eocene to  
148 Oligocene bedded meta-volcanics, meta-sediments, and basaltic to andesitic flow deposits of  
149 the Caraballo Formation. Coarse crystalline diorite intrusions that are possibly from the  
150 Dinalungan Diorite Complex are also noted within the region (Mines and Geosciences Bureau,  
151 2010). Late Pliocene to Early Pleistocene conglomerates consisting of andesite porphyry  
152 clasts of the Ilagan formation are also observed along the Ilagan River.

153

154

155



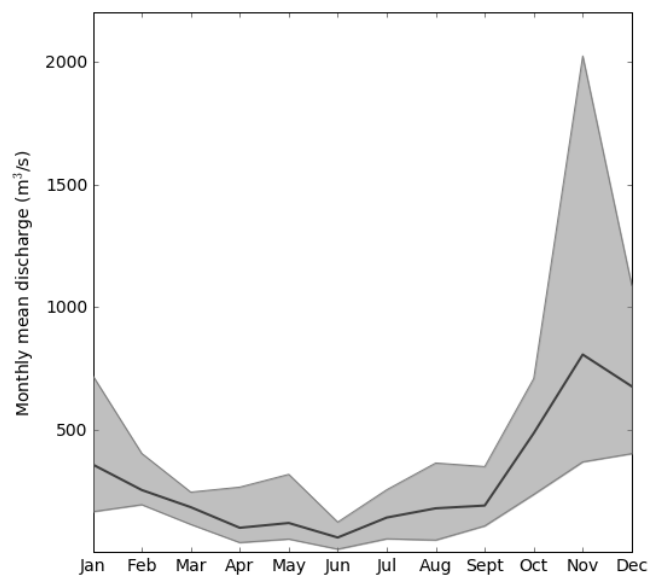
156

157 Fig. 1. a) Location of Luzon Island and the Cagayan basin. The Ilagan, Abuan and Bintacan  
 158 boundaries are shown in black. The study area is denoted by the red box. b) Study area and surface  
 159 grain size measurement sites (yellow stars). Coordinates are projected in UTM Zone 51N.

160

161 The Pinacanauan de Ilagan River catchment experiences relatively subdued seasonality  
 162 (Tolentino et al., 2016), but monthly discharge data shows a drier period between November  
 163 and April (Fig. 2). Modelled water balances under a range of future climate scenarios across  
 164 the Philippines have suggested an overall increase in annual water availability, with the  
 165 proportionally largest increases in peak river runoff predicted for catchments on Luzon Island

166 (Tolentino et al., 2016). This northern region of Luzon Island experiences several typhoons  
167 each year (generally between October-January, Fig. 3), generating significant overbank  
168 flooding and damage to local communities (Rojas, 2014). These short-lived (~24 to 48 hour),  
169 high magnitude flows (>10,000 m<sup>3</sup>/s) (Fig. 3) also generate and transport large quantities of  
170 sediment from the Sierra Madre mountains, driving channel bed aggradation and bank erosion  
171 further downstream where lower gradient and laterally extensive floodplains have developed.  
172



173  
174 Fig. 2. Mean monthly discharge between 1985 and 2010 for the Pinacanauan de Ilagan River at Ilagan  
175 City, where maximum and minimum monthly averages are shown by the grey envelope.

176  
177  
178  
179  
180  
181



182  
183  
184  
185  
186  
187  
188  
189  
190  
191  
192  
193  
194  
195  
196  
197  
198  
199  
200  
201  
202  
203  
204  
205  
206  
207  
208

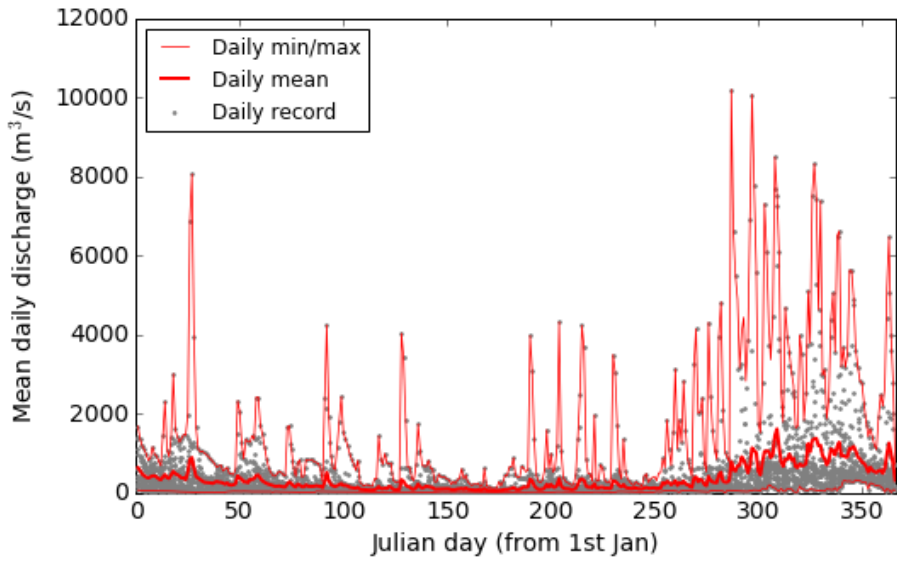
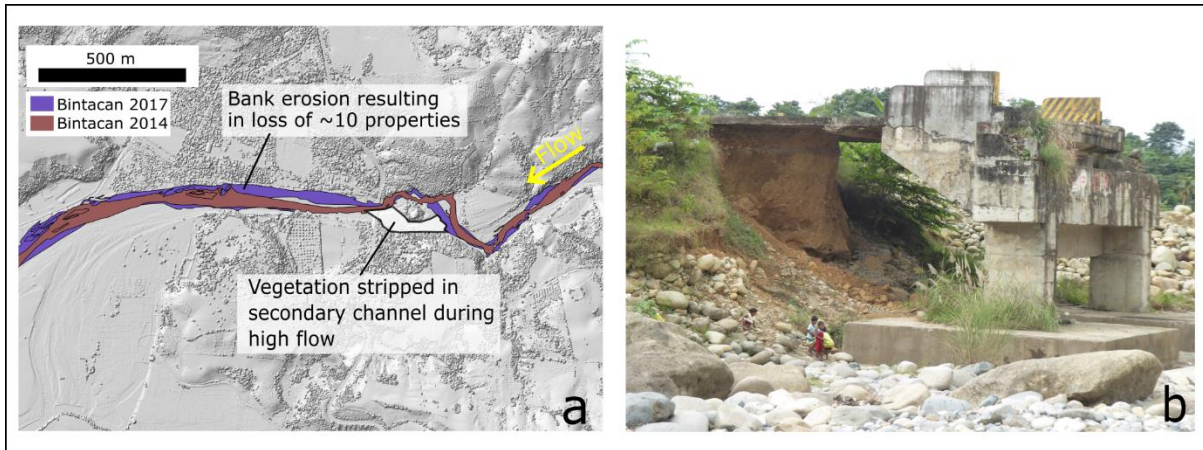


Fig. 3. Measured mean daily discharge (grey dots) at Ilagan, 1985-2010. Daily minima and maxima are shown in thin red lines, whilst the mean value for each calendar day over the entire period is shown by the thicker red line.

Floodwaters generated by Typhoon Lawin (in 2016) in the Bintacan and Abuan catchments mobilised substantial quantities of coarse sediment from the catchment headwaters. These coarse sediments were subsequently deposited in the lower reaches of the Bintacan and Abuan catchments driving lateral bank erosion, loss of floodplain and channel re-organisation. Locally, this resulted in the loss of ~10 properties due to bank erosion along the Bintacan River, as well as damage to transport infrastructure (Fig. 4). Changes in channel bed elevation driven by sediment deposition in the lower reaches of the catchment are also likely to compound flood risk where the gradient of the landscape is very low and tributary confluences are closely spaced. Changes in the base level of either the tributaries or the main river may also influence the backwater length and water depths at channel confluences (Samuels, 1989; Ferguson et al., 2006).



209

210 Fig. 4. a) Lateral erosion of the Bintacan channel in response to Typhoon Lawin (2016), resulting in the  
 211 loss of several properties on the right bank, destruction of the road bridge, and significant reworking  
 212 and transport of coarse sediment through the reach. The brown shading represents the channel position  
 213 in 2014 whilst the purple represents the 2017 channel. b) Example of infrastructure damage caused by  
 214 Typhoon Lawin on the Bintacan channel (17°07'12.83"N, 122°00'41.60"E) where a major road bridge  
 215 was destroyed and significant coarse sediment deposition occurred.

216

217 2. Methods

218

219 2.1. Channel and confluence migration

220

221 Sediment exchange between the channel and floodplain can form a substantial component of  
 222 modern river sediment loads. For example, sediment budget estimates derived from optical  
 223 satellite images and <sup>210</sup>Pb geochronology along the Strickland River in Papua New Guinea  
 224 suggested that floodplain recycling could account for as much as 50% of the total river  
 225 sediment load (Aalto et al., 2008). Here, we quantify rates of confluence and lateral channel  
 226 migration using satellite imagery spanning the past ~40 years from Landsat and Sentinel-2  
 227 satellite missions (see Table S1 for details).

228

229 The positions of major channel confluences across the study area were identified from each  
 230 scene to examine and quantify patterns of confluence migration, the drivers of which are

231 broadly similar to those driving lateral channel migration (Dixon et al., 2018). Where systems  
232 have high sediment supply, easily erodible floodplains and variable discharges (e.g.,  
233 monsoon-dominated climates), large river confluences can be highly mobile (Best and  
234 Ashworth, 1997; Dixon et al., 2018). Confluences of interest were limited to those with  
235 channels wide enough (>60 m) to be clearly identified on older satellite images with lower  
236 spatial resolution; these included the Cagayan-Ilagan, Abuan-Ilagan and Bintacan-Ilagan  
237 confluences.

238

239 Lateral channel migration rates were calculated from manually digitising channel bank  
240 positions from imagery captured in 1973, 1990, 2001, 2008 and 2017. This analysis has been  
241 restricted to the Ilagan and Cagayan channels within the study area, as lower resolution  
242 imagery from earlier Landsat missions was too coarse to distinguish either the smaller Abuan  
243 or Bintacan channels. Channel centerlines and lateral migration rates of individual meander  
244 bends were then calculated in ArcGIS 10.4 using the Stream Restoration Toolbox (Planform  
245 Statistics Tool) described in Aalto et al. (2008).

246

## 247 2.2. Channel pattern

248

249 Channel pattern has been strongly correlated with upstream sediment supply (e.g., Schumm,  
250 1985; Miller and Benda, 2000; Church, 2006; Eaton et al., 2010). As sediment supply to a  
251 single-thread channel increases, a response in channel pattern is likely to occur (i.e. transition  
252 from single-thread to braided) (Mueller and Pitlick, 2014). The more dynamic nature of braided  
253 channels allows the system to maintain equilibrium transport conditions under higher sediment  
254 supply conditions (Leopold and Wolman, 1957; Smith and Smith, 1984; Eaton et al., 2010;  
255 Mueller and Pitlick, 2014), where braided channels are more commonly associated with  
256 physiographic settings with steeper channel gradients and higher runoff that yield high stream  
257 power compared to single-thread meandering channels (Ashmore, 2013). As such, changes  
258 in channel pattern may reflect changes in sediment supply, or channel gradient, within the

259 Ilagan catchment. Channel sinuosity and braiding intensity were then assessed using  
260 GoogleEarth imagery by comparing the down-valley and channel centreline distances  
261 between two points, and the total length of all braid channels relative to the length of the  
262 channel thalweg between two points (Mosley, 1981), respectively. Points or reaches were  
263 spaced where distinct changes in channel morphology could visually be distinguished along  
264 continuous reaches (e.g., transitioning from confined to unconfined floodplain conditions), or  
265 at channel confluences. In addition to the Pinacanauan de Ilagan River, channel pattern was  
266 also assessed further downstream along the full length of the Cagayan River. The confined  
267 bedrock portions of the Bintacan and Abuan catchments were not considered.

268

269 Transitions from single-thread to braided reaches can also be caused by lateral valley  
270 constriction (which initiates bed aggradation) or changes in sediment grain size delivered from  
271 tributaries (Mueller and Pitlick, 2014), in addition to changes in channel slope (e.g., Leopold  
272 and Wolman, 1957; Van den Berg, 1995; Dade, 2000). For comparison with previous studies,  
273 a dimensionless discharge ( $Q^*$ ) (Parker, 1979; Eaton et al., 2010; Mueller and Pitlick, 2014)  
274 is defined as

275

$$276 \quad Q^* = \frac{Q_{bf}}{(\sqrt{(s-1)gD_{50}})D_{50}^2} \quad [1]$$

277

278 where  $D_{50}$  is the median grain size from each sampling location,  $Q_{bf}$  is bankfull discharge ( $m^3/s$ )  
279 and  $(s-1)$  is the submerged specific gravity of the sediment. Reach slopes were taken as  
280 averages over 10 km, this length being chosen to reduce the effect of artificial noise from the  
281 airborne IfSAR (interferometric synthetic aperture radar) DEM (acquired in 2013), as  
282 calculation of very low gradients can easily be biased by artificial steps in the topographic data.  
283 Bankfull discharge estimates of 2000, 800 and 4000  $m^3/s$  were made for the Abuan, Bintacan  
284 and Ilagan channels, respectively, by Rojas (2014) using preliminary hydrological modelling.  
285 These bankfull discharge values are conservatively varied by  $\pm 50\%$  in our calculations of  $Q^*$

286 to account for uncertainty in these estimates. Rainfall-runoff modelling predictions by McMillan  
287 et al. (2010) suggested that simulations of flood peaks can be under-estimated by almost 50%  
288 in these types of models. Dimensionless discharge values were then plotted against channel  
289 gradient at each grain size sampling location and compared to previously published data  
290 (Mueller and Pitlick, 2014) to examine whether observed channel patterns match predicted  
291 patterns based on the published relationships between channel slope, bankfull discharge,  
292 sediment grain size and bank strength (Eaton et al., 2010; Mueller and Pitlick, 2014). Using  
293 these data, it is possible to examine whether changes in channel planform are related to  
294 changes in sediment supply across the Ilagan catchment.

295

### 296 2.3. Channel width

297

298 Discharge ( $Q$ ) is typically related to channel width ( $w$ ) by a relationship of the form  $w \propto Q^b$   
299 (e.g., Leopold and Maddock, 1953; Church, 1992; Wobus et al., 2006) where the exponent  $b$   
300 ranges between 0.3-0.6, although few previous studies have specifically focused on tropical  
301 river systems. Bankfull width was measured at eight transects spaced 100 m upstream and  
302 downstream of 16 tributary junctions across a range of rivers within the Cagayan catchment  
303 that were wide enough ( $>100$  m) to have errors of  $<10\%$  in making measurements from the  
304 remote sensing images. Measurements were made from a combination of Sentinel 2 and  
305 RapidEye satellite images and excluded mid-channel bars which were densely vegetated and  
306 therefore unlikely to be submerged for extensive periods (details in Table S1). Average  
307 upstream ( $w_u$ ), downstream ( $w_d$ ) and tributary ( $w_t$ ) widths were calculated from these  
308 measurements at each site. Following Ferguson and Hoey (2008), changes in channel width  
309 at tributary junctions are predicted from hydraulic geometry relationships as;

310

$$311 \quad w_d = w_u [1 + (w_t/w_u)^{1/b}]^b \quad [2]$$

312

313 where  $b = 0.5$  (e.g., Leopold and Maddock, 1953; Richards, 1980; Church, 1992). Solving  
314 equation [2] provides predicted downstream channel widths ( $w_{pd}$ ) using measurements of  $w_u$   
315 and  $w_t$  at each of the sixteen tributary junctions;

316

$$317 \quad w_{pd}^2 = w_u^2 + w_t^2 \quad [3]$$

318

#### 319 2.4. Sediment grain size

320

321 Surface sediment grain size distributions were collected along the Ilagan, Bintacan and Abuan  
322 channels on exposed gravel bar heads at low flow using Wolman counts in January 2018  
323 (Wolman, 1954) on sample sizes of ~300 at each site to ensure precision of the order of  $\pm 0.1 \psi$   
324 units for  $D_{50}$ , where  $2^\psi = D$  (Rice and Church 1996; Fig. 1).

325

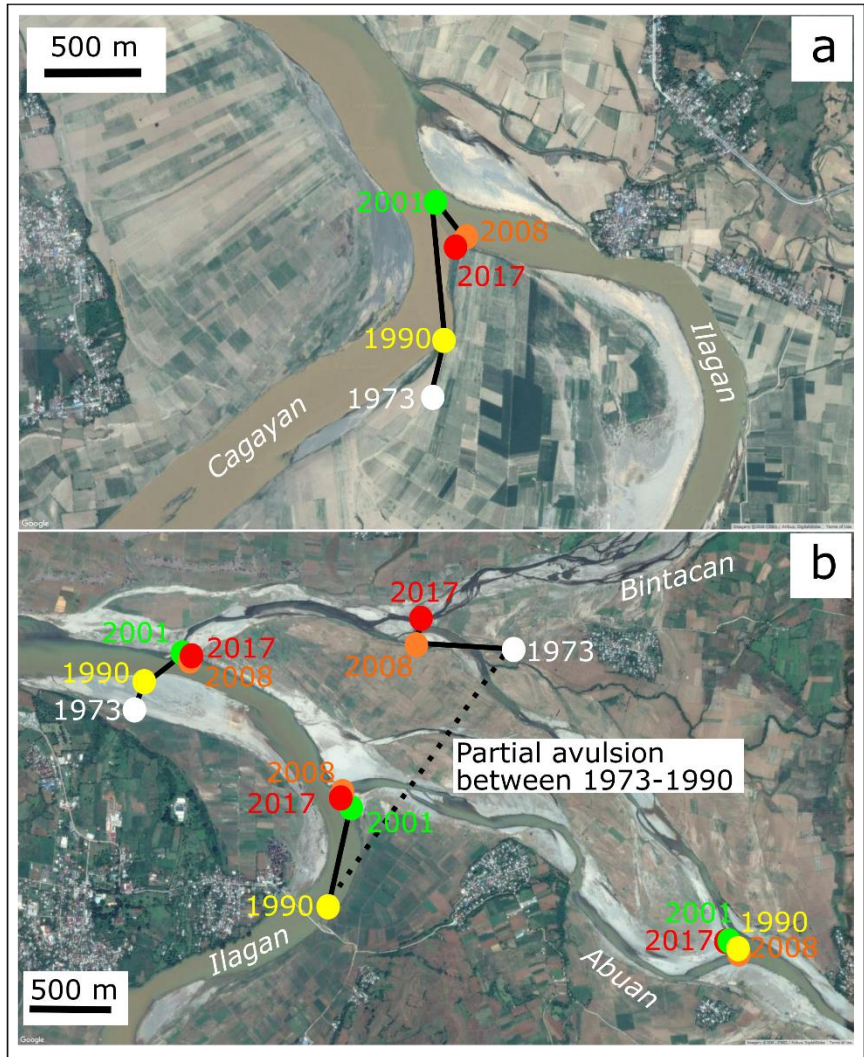
### 326 3. Results

327

#### 328 3.1. Lateral channel and confluence migration

329

330 A number of channel confluences within the Ilagan catchment were highly mobile between  
331 1973 and 2017, migrating net distances of more than a kilometre over this ~40-year period.  
332 Patterns of confluence node migration for the three most mobile confluences are shown in Fig.  
333 5. Between 1973 and 1990 a partial avulsion also occurred on the Abuan forming a new  
334 channel between the Abuan and Bintacan rivers, approximately 2-3 km upstream of their  
335 respective confluences with the Ilagan channel.



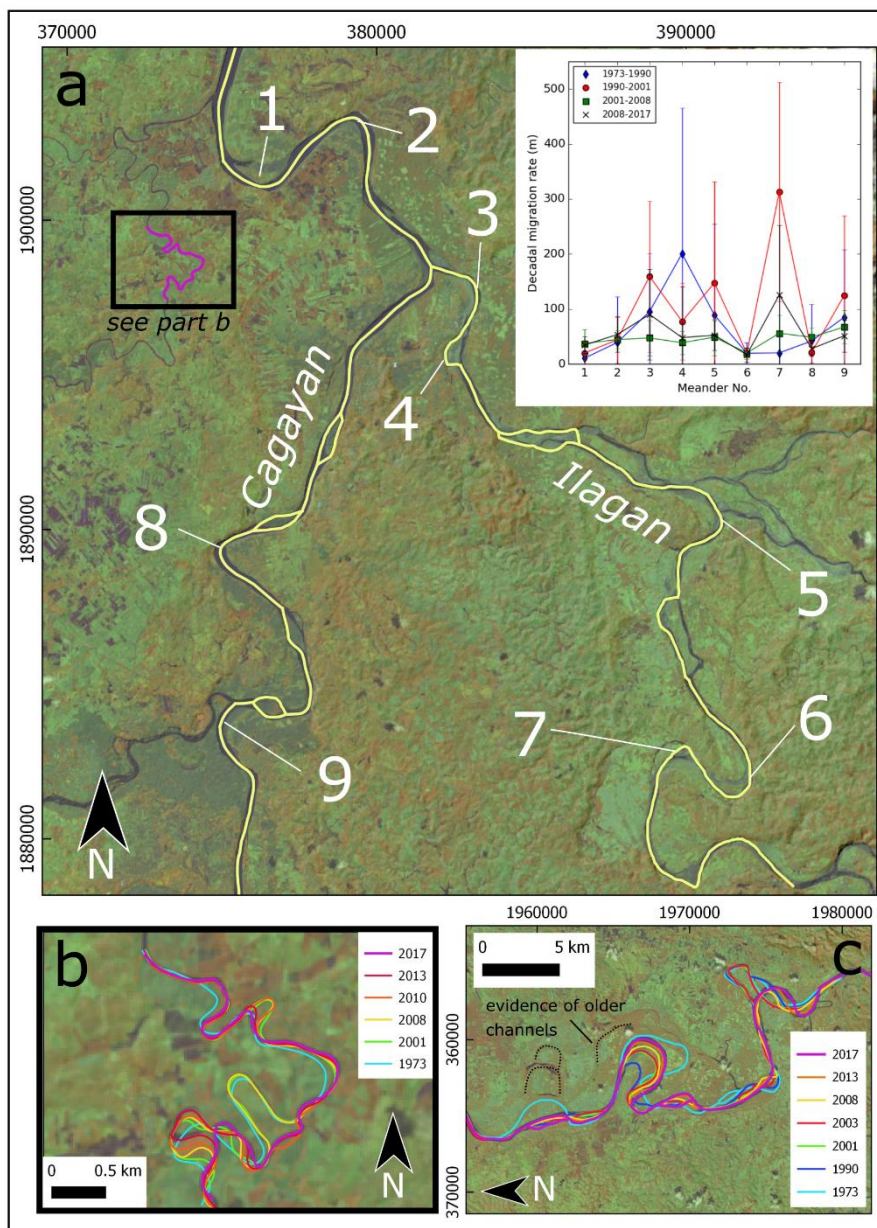
336

337 Fig. 5. a) Patterns of confluence node migration between 1973 and 2017 at the Cagayan-Ilagan  
 338 confluence; and, b) at the Bintacan and Abuan confluences with the Ilagan channel. In 1973, the Abuan  
 339 channel discharged into the Bintacan channel rather than directly into the Ilagan. A partial avulsion  
 340 occurred between 1973 and 1990, however, such that the Abuan can now discharge directly into the  
 341 Ilagan. The base maps for both images are from 2017 in GoogleEarth.

342

343 Channel migration rates averaged over four time periods between 1973 and 2017 are shown  
 344 in Fig. 6a. These rates have been normalised to decadal averages based on the differing time  
 345 intervals between available images, which spanned from 7 (2001-2008) to 17 (1973-1990)  
 346 years. In general, the highest decadal migration rates were observed at meander numbers 3,  
 347 4, 5, 7 and 9 with the period 1990-2001 showing the highest rates (over 300 m per decade at

348 meander 7). High rates of lateral meander migration are observed for channels across a range  
 349 of spatial scales, from highly sinuous smaller tributaries where meander cut-offs are also  
 350 prevalent (Fig. 6b), to the larger Cagayan River further downstream where meander migration  
 351 has occurred at kilometre scale between 1973-2017, and older palaeo-channels are preserved  
 352 considerable distances (~5 km) away from the modern channel (Fig. 6c). Lower meander  
 353 migration rates at meanders 1, 2, 6 and 8 may relate to local confinement of the channel where  
 354 the valley bottom is topographically constricted (Fig. 7a), which will inhibit significant lateral  
 355 migration.  
 356



357



358 Fig. 6. a) Lateral channel migration rates for individual meanders (numbered 1-9) derived using methods  
359 described in Aalto et al. (2008). Rates calculated between images have been normalised to decadal  
360 migration rates where the marker represents the average migration rate of the entire meander, and  
361 error bars represent +/- 1 standard deviation in rates calculated for each reference point around the  
362 individual meander. The base map and yellow centreline represents the 2017 channel position. The  
363 extent of this study area is shown by the red box on Fig. 1a. b) Channel positions between 1973 and  
364 2017 for a small tributary of the Cagayan, where the location is shown by a black box in part a. c)  
365 Channel positions between 1973 and 2017 along the larger Cagayan system further downstream of  
366 Ilagan City. Meander scarps and evidence of kilometre scale channel migration (chute cut-off) prior to  
367 1973 are clearly visible across the Cagayan Valley.

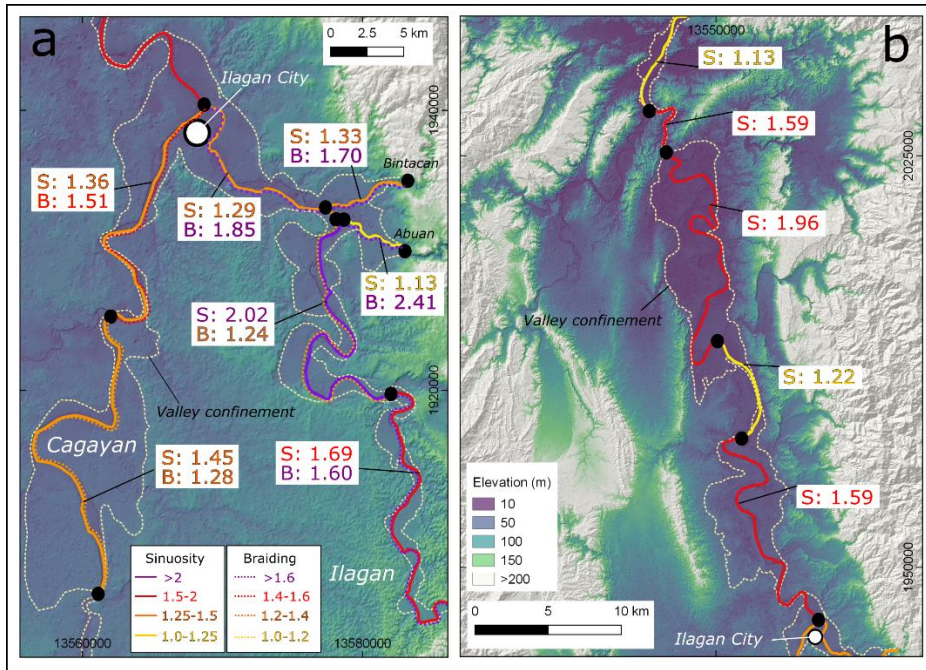
368

### 369 3.2. Channel pattern

370

371 Sinuosities calculated from GoogleEarth imagery (captured in June 2017) are generally  
372 highest upstream of the Bintacan and Abuan confluences in the Ilagan channel (2.02 and 1.69)  
373 (Fig. 7a). Where the Bintacan and Abuan channels exit their confined channels in the Sierra  
374 Madre mountains, braiding intensity is also relatively high, as aggradation occurs in response  
375 to the lower channel gradient and loss of lateral confinement. Where these two tributaries  
376 enter the Ilagan channel, channel sinuosity decreases from 2.02 to 1.29 and braiding intensity  
377 increases from 1.24 to 1.85 (Fig. 7a). These changes are consistent with an increase in  
378 sediment supply to the Ilagan channel from the Bintacan and Abuan tributaries. In comparison  
379 to the Ilagan channel upstream of the Cagayan-Ilagan confluence at Ilagan City, the Cagayan  
380 River is generally slightly more sinuous, and is essentially single-thread. Downstream of the  
381 Cagayan-Ilagan confluence, channel sinuosity increases along the Cagayan River (Fig. 7b).  
382 Braiding intensity was not calculated along the main Cagayan River as the channel is  
383 essentially single-thread.

384

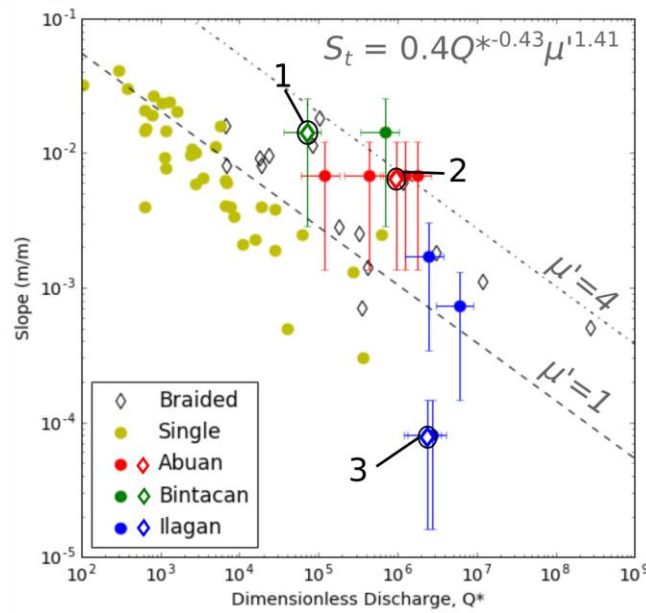


385

386 Fig. 7. a) Channel sinuosity (solid line) and braiding intensity (dashed line) on the Ilagan, Bintacan and  
 387 Abuan channels upstream of Ilagan City. b) Channel sinuosity on the Cagayan between Ilagan City and  
 388 the Cagayan delta. In both figures, yellow lines represent the lowest sinuosity (and braiding intensity),  
 389 purple lines represent the highest and orange and red colours represent intermediate values (shown in  
 390 the key on panel a). The extent of the valley floor or floodplain (valley confinement) is also shown for  
 391 each panel, and was determined by where either a break or change in valley bottom slope was  
 392 observed.

393

394



395

396 Fig. 8. Dimensionless discharge,  $Q^*$ , plotted as a function of channel slope,  $S$ . Braided and single-  
 397 thread channel data from a global compilation of rivers presented in Mueller and Pitlick (2014) are  
 398 shown in black outlined diamonds and filled yellow circles, respectively. New data from this study are  
 399 shown by coloured solid circles (single-thread) and outlined diamonds (braided). Horizontal error bars  
 400 represent  $Q^*$  generated by varying bankfull discharge by  $\pm 50\%$ , and vertical error bars represent slope  
 401 within  $\pm 80\%$  of the value calculated from the DEM. Dashed lines represent the relationship between  $S_t$   
 402 (the threshold slope between braided and single-thread channels) and  $Q^*$  from Eaton et al. (2010) used  
 403 to differentiate braided from single-thread channels, using two different dimensionless relative bank  
 404 strength ( $\mu'$ ) values of 4 and 1. Highlighted data points (labelled 1, 2, and 3) relate to samples collected  
 405 during this study from braided channels, where all other points are from single-thread reaches.

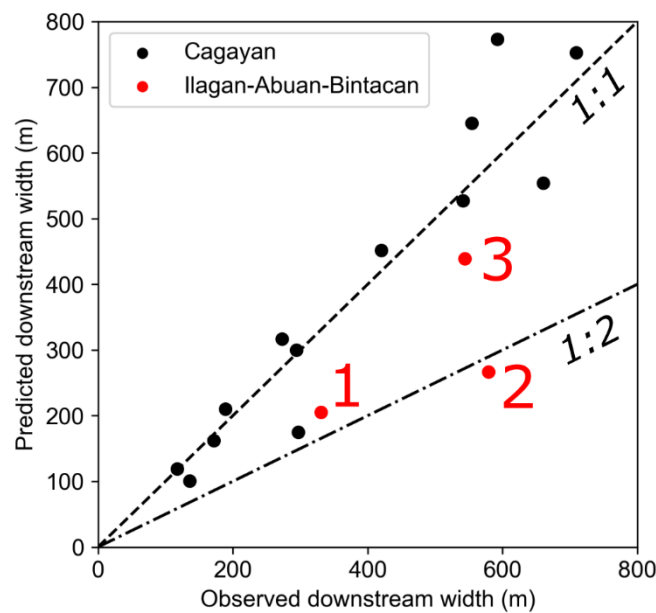
406

407 Previous studies have found relationships between dimensionless discharge, channel slope  
 408 and channel pattern (e.g., Eaton et al., 2010; Mueller and Pitlick, 2014), but the Ilagan, Abuan  
 409 and Bintacan channels are inconsistent with these result (Fig. 8). Only two of the three braided  
 410 sites were consistent with previous measurements of braided channels (labelled 1 and 2 on  
 411 Fig. 8), whilst the single-thread channel sites did not conform with the relationship of Eaton et  
 412 al. (2010) except when the dimensionless relative bank strength was set to relatively high  
 413 values of  $\sim 4$ . For the upstream Bintacan and Abuan samples where the channel was still  
 414 confined and exposed bedrock was present, these relative bank strength values are more

415 reasonable. Even when varying the bankfull discharge estimates by  $\pm 50\%$  (the parameter with  
 416 the most uncertainty), a number of the samples are still not consistent with the threshold  
 417 proposed from the the global dataset in Mueller and Pitlick (2014). By varying channel slope  
 418 by  $\pm 80\%$  of the values derived from the IfSAR DEM, the errors bars indicate there is some  
 419 overlap with the Mueller and Pitlick (2014) dataset and braided to single-thread threshold.

420

421 3.3. Channel width



422

423 Fig. 9. Predicted and observed variations in channel width downstream of tributary junctions across  
 424 the Cagayan catchment. The three red points relate to tributary junctions within the study area; 1)  
 425 Upper Ilagan (near grain size site C1 on Fig. 1), 2) Bintacan-Ilagan (near grain size site C3), 3)  
 426 Cagayan-Ilagan (near grain size site C4). The black dashed lines represent 1:1 and 1:2 relationships  
 427 between observed and predicted channel width.

428

429 The Cagayan channel width data show a strong positive relationship between predicted and  
 430 observed channel width (Fig. 9), suggesting that width scales proportionally with discharge  
 431 and favours the use of  $b = 0.5$  which was initially derived from observations in temperate  
 432 systems (Leopold and Maddock, 1953; Ferguson and Hoey, 2008). Values which deviate from

433 this trend represent values where the observed channel width is generally greater than the  
434 predicted value, as is evident in the three tributary junctions associated with the Cagayan-  
435 Ilagan-Bintacan region (shown in red).

436

#### 437 3.4. Sediment grain size

438

439 Sediment sizes in the main Ilagan channel are typically finer than those in either the Abuan or  
440 Bintacan tributaries (Fig. 10). Grain sizes in the Abuan and Bintacan are more variable, both  
441 within each sample where the sorting  $(D_{84}/D_{16})^{0.5}$  is poorer, and spatially across the sampled  
442 bars than in the main Ilagan channel. This variability and poor sorting are consistent with field  
443 observations of coarser lateral inputs of sediment directly from adjacent hillslopes into these  
444 channels, and also that tributaries to these rivers are steep and laterally confined within the  
445 Sierra Madre mountains. In contrast, the Ilagan channel flows largely through a lower gradient  
446 and unconfined alluvial plain. The grain sizes measured furthest downstream on the Abuan  
447 and Bintacan channels ( $D_{84} = 75.6$  and  $74.1$  mm, respectively) are comparable to that of the  
448 Ilagan channel ( $D_{84} = 81.2$  and  $80.1$  mm for sites Ilagan 2 and 3, respectively).

449

450

451

452

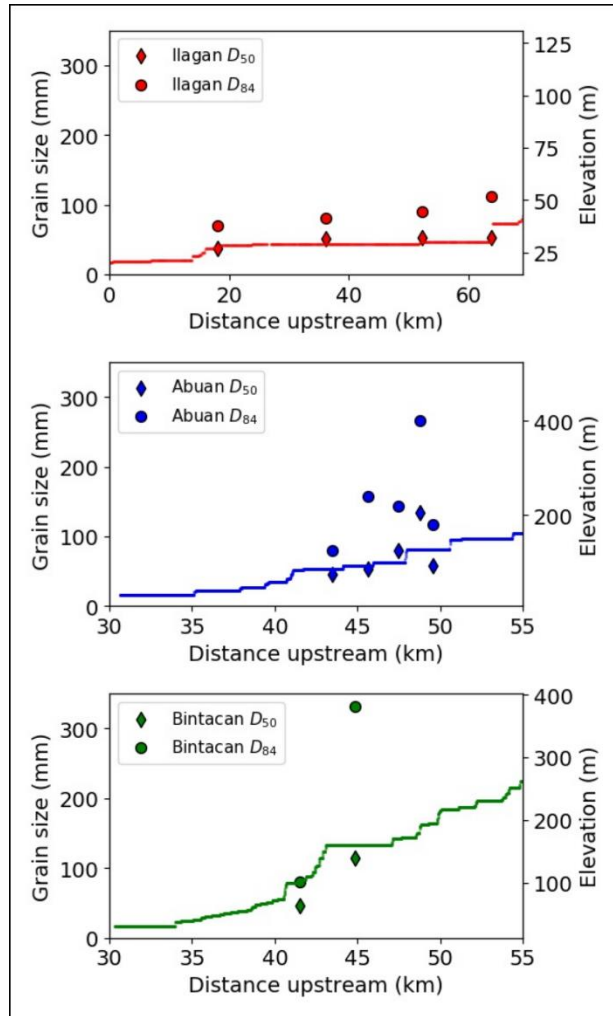
453

454

455

456

457



458

459 Fig. 10.  $D_{50}$  and  $D_{84}$  grain size statistics from surface grain size measurements on the Ilagan, Abuan  
 460 and Bintacan channels (locations shown in Fig. 1b). Long channel profiles are also shown for each  
 461 system, where the distance upstream is relative to the most downstream location of the study area (on  
 462 the Ilagan channel).

463

464 **4. Discussion**

465

466 4.1. Impact of catchment disturbance on sediment supply and transport in the Cagayan  
 467 catchment

468

469 Between 1987 and 2010, from analysis of satellite imagery, approximately 14% of the Isabella  
 470 province is suggested to have undergone deforestation (Forest Management Bureau, 2013).

471 Forest clearance for agricultural land on the lower gradient Ilagan floodplain is likely to have  
472 caused a reduction in bank shear strength and cohesion; this reduction may have resulted in  
473 increased rates of lateral channel migration in this part of the catchment. Changes in forest  
474 cover are less well documented in the headwaters of the Ilagan catchment where access is  
475 limited but illegal logging is reported (van der Ploeg et al., 2011), suggesting that this process  
476 may also be important further upstream but more difficult to quantify. Sediment generated and  
477 transported by typhoon storms and their associated discharges in the Bintacan and Abuan  
478 catchments, however, were observed in thick (>5 m) sedimentary deposits which persist along  
479 channel margins within the Sierra Madre mountains. Sediment generated by the mass-wasting  
480 of hillslopes, triggered by typhoon storm events, appears to be the dominant mechanism  
481 through which sediment is supplied to these rivers, rather than changes in forest cover. This  
482 is consistent with findings from other tropical systems such as the LiWu River (Taiwan) where  
483 cyclone-induced floods are thought to drive 77-92% of non-fossil particulate organic carbon  
484 erosion and transport through the catchment (Hilton et al., 2008). When considered alongside  
485 an absence of systematic change in lateral migration rates across the region over the last ~40  
486 years (Fig. 6), there is no evidence that increased deforestation (over the same time period)  
487 in the Pinacanauan de Ilagan catchment has had any significant impact on channel  
488 morphodynamics.

489

#### 490 4.2. Sediment dynamics in the Pinacanauan de Ilagan catchment

491

492 On exiting the mountains, the Ilagan, Abuan and Bintacan all cross lower gradient alluvial  
493 plains where in many instances coarse boulders can be observed on the surface of much finer  
494 gravel bars. Large boulders (intermediate axes >1 m in some instances) observed on the  
495 Bintacan close to site B2 were attributed to the most recent Typhoon Lawin (2016), which  
496 generated sufficient discharge to transport boulders of this size several kilometres  
497 downstream onto the alluvial plain. However, the  $D_{50}$  and  $D_{84}$  grain size measurements at sites  
498 B2 and A5 were comparable to sites upstream and downstream of their confluences with the

499 Ilagan River (sites C2 and C3, respectively). This suggests that coarsest sediment generated  
500 in the Sierra Madre mountains is largely contained either within the confined bedrock channels  
501 or on the part of the alluvial plain that is immediately downstream of the exit from the mountains.

502

503 Increased braiding intensity immediately downstream of the Abuan and Bintacan confluences  
504 with the Ilagan is consistent with increased sediment supply to the Ilagan from these  
505 tributaries. Finer sediment generated by typhoon-induced hillslope failure, or by reworking of  
506 existing sedimentary deposits under high discharge conditions, is likely transported from the  
507 Sierra Madre mountains by the Bintacan and Abuan channels and deposited on entering the  
508 larger Ilagan channel. This is consistent with the abrupt reduction in channel gradient between  
509 the tributaries and main Ilagan channel (Fig. 10), which would result in the rapid deposition of  
510 sediment which is too coarse to be entrained in the Ilagan channel.

511

512 4.3. The role of topographic constraints and channel aggradation on channel pattern, width,  
513 and migration

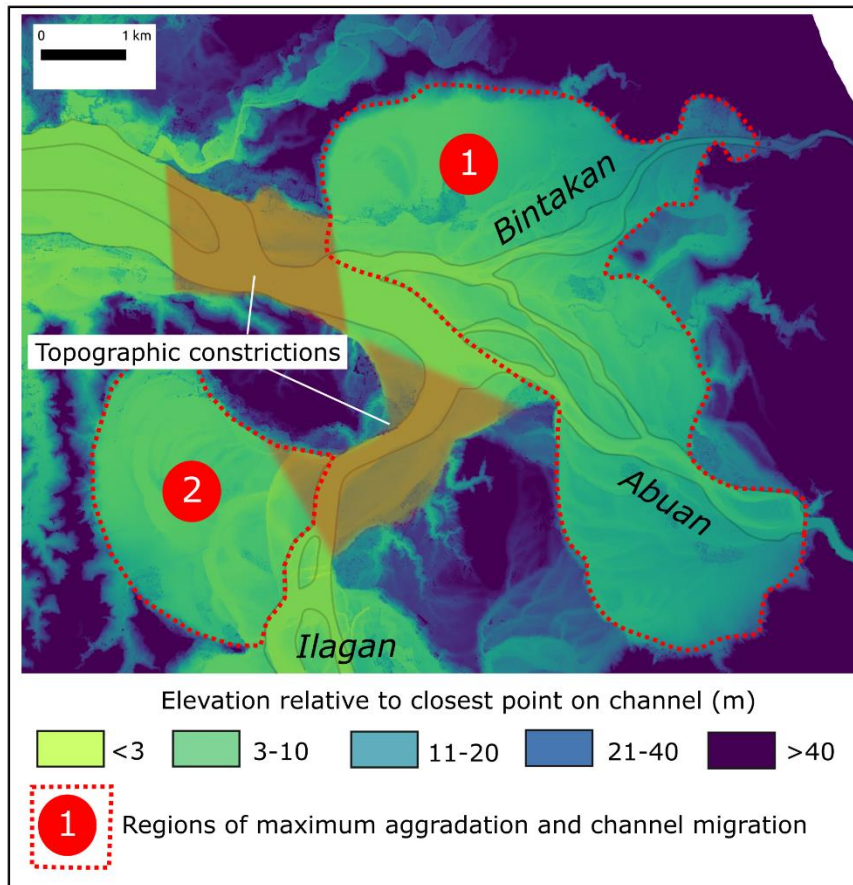
514

515 Sediment deposition or aggradation in the confluence region is likely to be enhanced by local  
516 topographic constriction of the channel immediately upstream and downstream of the tributary  
517 confluences (Fig. 11). Following the methodology of Clubb et al. (2017), swath profiling of the  
518 Ilagan-Abuan-Bintacan area using 1 m resolution LiDAR data highlights patterns of  
519 topographic relief and channel migration in the region, where landscape elevation is  
520 normalised to the elevation of the closest point on the river channel (Hergarten et al., 2014;  
521 Dingle et al., 2016; Clubb et al., 2017). Broad alluvial plains with numerous scroll bars and  
522 meander scarps can be seen immediately upstream of each zone of channel constriction,  
523 suggesting that rates of channel migration and reworking are substantially enhanced in these  
524 regions. Relatively high channel sinuosities and reduced braiding intensity on the Ilagan  
525 upstream of the Abuan confluence may be a response of the Ilagan channel to enhanced bed  
526 aggradation (caused by the topographic constrictions) and a subsequent narrowing of the



527 channel, forcing the channel to incise into these deposits. Interestingly, a similar pattern is  
528 observed further downstream on the Cagayan River (Fig. 7b) where channel sinuosity is  
529 considerably higher in regions immediately upstream of topographic constrictions. The  
530 prevalence of meander scarps and chute cutoffs across these regions also supports high rates  
531 of lateral channel migration. In the reach between the two lateral constrictions identified on  
532 Fig. 10, the high sediment inputs from the Bintacan and Abuan tributaries prevent the channel  
533 from incising into the alluvial floodplain. Instead the braiding intensity and rates of confluence  
534 and channel migration are elevated, resulting in more rapid recycling and reworking of the  
535 alluvial floodplain, where vertical incision is inhibited by higher rates of aggradation on the  
536 channel bed. Along the Cagayan and Ilagan Rivers, valley confinement is closely related to  
537 channel pattern and lateral channel migration rate. Regions upstream of these topographic  
538 constrictions typically have more sinuous channel planforms and undergo higher rates of  
539 lateral channel migration as a result of locally increased aggradation (due to high sediment  
540 supply). Channels incise into the alluvial plain in order to reduce their gradient, and once  
541 developed, migrate laterally in order to maintain channel capacity as sediment is transported  
542 and deposited within the reach. Where rates of bed aggradation are very high, the channel  
543 may not be able to incise vertically and, instead, braiding intensity remains high and the  
544 channel belt (and floodplain) is rapidly reworked by a series of smaller braids or channels. In  
545 contrast, as single-thread channels pass through confined regions they are more laterally  
546 stable as lateral adjustment is inhibited by high relative bank strength. The sinuosity of these  
547 confined reaches is more likely to be a function of the valley topography than flow or sediment  
548 dynamics.

549



550

551 Fig. 11. Swath profile of the Ilagan-Abuan-Bintakan confluence region, highlighting the local distribution  
 552 of topographic relief and lateral channel and floodplain constrictions. Elevation (shown by colours) is  
 553 normalised to the elevation of the closest point on the channel. Two zones delineated by red dashed  
 554 lines highlight parts of the floodplain upstream of lateral constrictions where numerous scroll bars and  
 555 meander scarps are evident, suggesting regions of enhanced lateral channel migration.

556

557 Comparing new meander migration rates from this study with existing rates in a number of  
 558 temperate and tropical rivers (both disturbed and undisturbed), the highest migration rates are  
 559 typically observed in larger catchments (Fig. 12). These rates are independent of channel  
 560 width and radius of meander curvature, which have been commonly used to non-  
 561 dimensionalise migration rates for channel and catchment size (e.g., Hickin and Nanson, 1975;  
 562 Hudson and Kesel, 2000; Hooke, 2007). In general, migration rates in tropical catchments for  
 563 a given catchment area exceed those in temperate regions. One temperate system with large  
 564 migration rates is the Lower Mississippi River (Hudson and Kesel, 2000) where meander

565 migration rates of up to 123 m/yr were observed pre-disturbance. However, although high  
 566 these rates are consistent with the relationship between catchment area and migration rate  
 567 (Fig. 12). The spatial variability in migration rates reported by Hudson and Kesel (2000) were  
 568 attributed to heterogeneity of floodplain deposits, where resistant clay plugs reduced migration  
 569 rates by forcing meander bends in these regions to develop more arcuate morphology.  
 570 However, the influence of variability in floodplain composition/channel bank strength (e.g., clay  
 571 versus poorly consolidated sand) was not considered in terms of wider channel morphology  
 572 and sediment transport dynamics, which may drive differences in aggradation and lateral  
 573 migration rates.

574

575

576

577

578

579

580

581

582

583

584

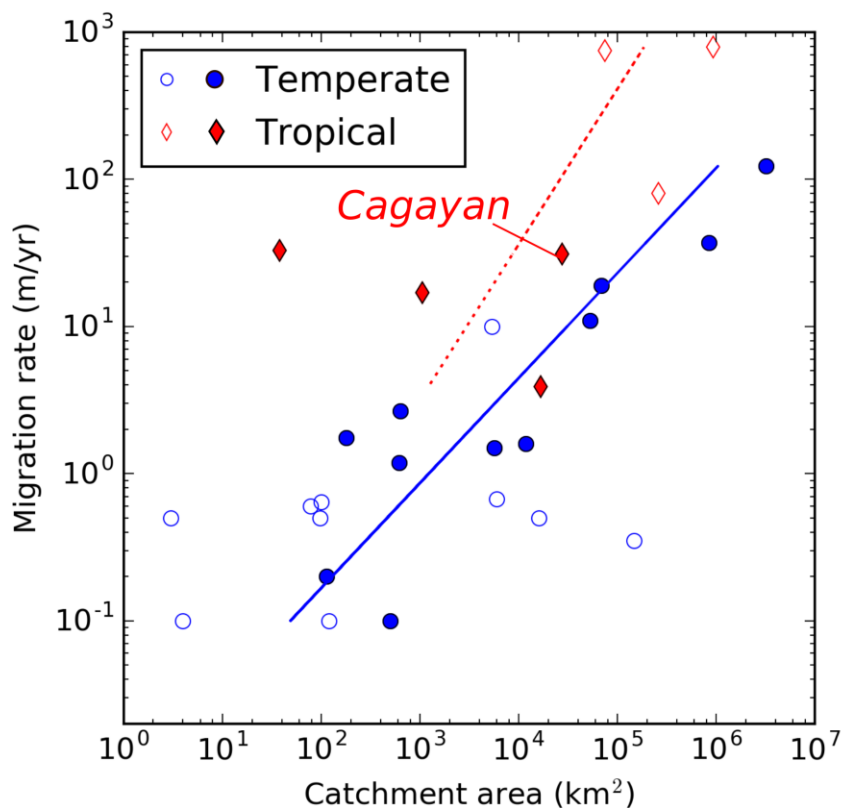
585

586

587

588

589



590 Fig. 12. Annual channel and meander migration rates from this and published studies (Wolman and  
 591 Leopold, 1957; Hooke, 1980; Lawler, 1993; Hudson and Kesel, 2000; Micheli et al., 2004; Horton et al.,  
 592 2017; Suizu and Nanson, 2018). Red diamonds represent data from tropical river systems, while blue  
 593 circles represent temperate river systems. It should be noted that these migration rates include a

594 combination of reach average and maximum meander migration rates, averaged over variable time  
595 periods. Where information was available, closed symbols represent maximum reported migration rates  
596 while open symbols represent a combination of mean migration rate or sources where it was not  
597 specified. Best-fit power relationships are also shown for both datasets (blue and red lines).

598

599 High aggradation rates in the Cagayan may also explain the disagreement between channel  
600 pattern, dimensionless discharge and channel gradient (Fig. 8) in comparison to global  
601 channel pattern data sets (e.g., Eaton et al., 2010; Mueller and Pitlick, 2014). Data from the  
602 single-thread Bintacan, Abuan and Ilagan channels suggest that very high relative bank  
603 strengths would be required to align with published relationships. Such high relative bank  
604 strength values are possible where the channel was laterally constrained by bedrock channel  
605 walls or very localised clay deposits within the channel bank. This suggests that using  
606 relationships such as Mueller and Pitlick's (2014) to predict channel pattern may not be fully  
607 appropriate in systems which transition between bedrock and alluvial settings where the  
608 channel is not always free to adjust its width, in systems responding transiently to changes in  
609 sediment supply, or where relative bank strength is highly variable (heterogeneous floodplain  
610 compositions). The presence of locally braided reaches suggests that many of these channels  
611 may be close to a threshold between single-thread and braided forms. The two data points on  
612 the Ilagan channel (labelled 3 on Fig. 8) based on measurements at sites C2 and C3, are also  
613 located around the Abuan and Bintacan channel confluences where aggradation rates may  
614 be periodically enhanced by high sediment inputs from these tributaries. As such, these sites  
615 may represent transient and non-regime responses to these aggradational conditions (Eaton  
616 et al., 2010). The relatively high recurrence interval of extreme sediment generating events  
617 in these headwater catchments, combined with spatial patterns of channel and valley  
618 confinement, are likely the dominant controlling factors on channel morphodynamics in the  
619 Cagayan valley.

620

621 Very few gravel-sized (or coarser) sediments were observed downstream of the Cagayan-  
622 Ilagan confluence. Grain size measurements made at location C4 were restricted to small  
623 patches of gravel exposed on the upstream end of a large sand bar. At the most downstream  
624 site on the Ilagan channel (C3), the channel is still dominated by gravel and larger sized  
625 sediments (Fig. 10). The simplest interpretation of this is that any coarse sediment delivered  
626 from the Ilagan into the Cagayan channel is rapidly buried by the comparatively larger sand  
627 flux transported by the Cagayan. Sand-bed conditions in the Cagayan may locally enhance  
628 transport of coarser sediment from the Ilagan tributary as a result of decreased bed roughness,  
629 allowing smaller patches of gravel (and coarser) sized sediments to persist in predominantly  
630 sand-bed channel conditions (Paola and Seal, 1995; Venditti and Church, 2014)

631

#### 632 4.4. Impact of observed morphodynamics for understanding tropical river geomorphology

633

634 Tributaries draining the Sierra Madre mountains generate and transport large sediment fluxes  
635 as a result of typhoon-induced hillslope mass wasting, which are likely to be enhanced by  
636 climatically-controlled chemical and biological processes (Syvitski et al., 2014). These  
637 processes include chemical weathering of bedrock and sediments, which may accelerate the  
638 breakdown or failure of hillslopes where rock strength (or fracture density) is weakened (or  
639 increased) by chemical processes such as dissolution. Similarly, high vegetation density in  
640 tributary headwaters may further accelerate chemical and physical weathering rates via  
641 processes such as tree throw and root pry (Gabet and Mudd, 2010) which both mechanically  
642 break down and remove rock and sediment, but also expose underlying bedrock to the  
643 atmosphere. Each year several high magnitude discharge events transport these large  
644 quantities of sediment efficiently through the Ilagan and wider Cagayan catchments. When  
645 combined with low gradient channels and poorly consolidated floodplain and bank sediments  
646 in the Cagayan Valley, these flood events and high sediment discharges appear to drive  
647 accelerated rates of lateral channel and confluence migration. In turn, this results in large

648 quantities of the Ilagan and Cagayan floodplain sediment being recycled back into the modern  
649 channels.

650

651 While the grain size of sediment observed in the Abuan and Bintacan tributaries was relatively  
652 coarse, the majority of this sediment does not appear to be exported downstream into the  
653 Ilagan or Cagayan channels. Any deposition of sediment delivered by the Abuan and Bintacan  
654 tributaries into the Ilagan is likely to enhance local rates of lateral erosion and floodplain  
655 reworking, as a result of reduced channel capacity, which would further accelerate the burial  
656 of coarser sediments. The high sediment loads delivered from these tributaries into the Ilagan  
657 and Cagayan may also explain the observed channel widening downstream of confluences in  
658 the study area (in comparison to other parts of the Cagayan catchment and data from  
659 temperate settings), where high aggradation rates immediately downstream of these  
660 confluences locally enhance lateral erosion and channel widening.

661

662 Increased lateral channel instability associated with the Abuan, Bintacan and Ilagan  
663 confluences initiates higher rates of sediment exchange between the entire modern Cagayan  
664 channel and floodplain further downstream. Where the channel is unconfined, the banks of  
665 the Cagayan River as it passes through the Cagayan valley are typically ~10-20 m thick, poorly  
666 consolidated sand and silt deposits which are unstable even under low to moderate flow  
667 conditions. Field observations confirm that many of these banks are severely undercut,  
668 commonly in the submerged portion of the bank (even under low flow conditions).  
669 Consequently, relatively low discharges may be capable of preconditioning or even driving  
670 bank collapse and erosion along the Cagayan River (Dunne and Jerolmack, 2018).

671

672 In actively migrating reaches, the exchange of floodplain-channel material is likely to be high  
673 enough that a large portion of the sediment load exported will have spent some time stored in  
674 the floodplain (Lauer and Parker, 2008). Patterns of channel migration and channel  
675 morphology are key in determining the timescales over which sediment resides within the

676 alluvial floodplain. In theory, periods of increased sediment supply (such as those driven by  
677 typhoon storms) will result in enhanced channel bed aggradation (and overbank  
678 sedimentation) upstream of topographically constrained reaches of the Ilagan catchment,  
679 driving an acceleration in channel reworking and lateral migration. The ability of the system to  
680 transfer this sediment, generated either directly by the event or by recycling of the alluvial  
681 floodplain, will be closely correlated to peak water discharges in subsequent months. In  
682 tropical river systems such as the Cagayan which experience numerous typhoons each year,  
683 high magnitude flow events occur frequently enough (Fig. 3) to efficiently both transport  
684 sediment downstream in either suspension or as bedload, and also laterally erode into alluvial  
685 banks so limiting excessive vertical aggradation of the channel bed. In regions where locally  
686 braided reaches exist and the channel is close to the threshold between braided and single-  
687 thread, these large sediment generating events may cause (temporary) changes in channel  
688 pattern until the channel is able to mobilise these deposits.

689

690 It is not possible at present to directly test whether sediment generated by high rates of  
691 floodplain recycling represents a significant proportion of the total sediment flux of the entire  
692 Cagayan catchment, as direct and reliable sediment concentration or flux measurements are  
693 not openly available. Data discussed in Principe (2012), based on monthly sediment yield data  
694 between 2002-2007 at Bangag monitoring station (close to the Cagayan outlet) were used to  
695 calibrate a SWAT (Soil and Water Assessment Tool) model of the Cagayan catchment which  
696 produced a simulated average sediment yield of 115 tonnes/ha/yr based on 2012 land use  
697 patterns. This sediment yield converts to an annual sediment flux of 317 Mt/yr, which is our  
698 only estimate of sediment flux for the Cagayan River. The yield can also be converted to a  
699 catchment-average denudation rate of 4.3-7.1 mm/yr, depending on the density of eroded  
700 material. This range of values is based on the density of quartz ( $2650 \text{ kg/m}^3$ ) and for  
701 uncompacted sand as might be expected across some of the Cagayan alluvial floodplain  
702 ( $1600 \text{ kg/m}^3$ ) and, as such, represents the widest range of possible values. Even the lower  
703 end of this range of values places the catchment-averaged denudation rate calculated here

704 among some of the highest rates from tectonically active mountain ranges globally  
705 (Montgomery and Brandon, 2002). Robust conclusions regarding the sediment budget of the  
706 Cagayan River are therefore difficult to make in the absence of openly available or spatially  
707 and temporally extensive sediment discharge gauging data. Syvitski et al. (2014) suggested  
708 that tropical rivers do not carry more particulate load to the oceans in comparison to more  
709 temperate systems, based on BQART modelling using average water discharge  
710 measurements. However, this modelling approach is likely to underestimate sediment flux  
711 where the annual sediment flux transport is dominated by short-lived, very high magnitude  
712 discharge events during typhoons.

713

#### 714 4.5. Consequences for river and flood risk management

715

716 The observed dynamism of channels in the study area suggests that sediment supply and  
717 channel migration are likely to change channel capacity and flow routing, and thus the  
718 associated flood and erosion risk to people, property and infrastructure. The area investigated  
719 here was chosen to be representative of catchments across the Philippines with similar  
720 characteristics. Our results imply that geomorphological change impacts flood risk, and that  
721 specific examples of this can be identified (Fig. 4). Our results show the significance of both  
722 aggradation and erosion, each of which has been identified as frequently being overlooked in  
723 flood risk management (Lane et al. 2007; Slater, 2016). Flood risk mapping in the Philippines  
724 has largely been undertaken as part of the Nationwide Operational Assessment of Hazards  
725 project (Lagmay et al., 2017) using two-dimensional hydraulic modelling over airborne-LiDAR  
726 derived topography. This approach has led to a step change in the understanding of flood risk  
727 but the existing modelling framework does not incorporate the impacts of topographic change  
728 on flood levels and routing. The results from this paper need to be extended to other  
729 catchments and can then be used to inform a national-scale assessment to identify river  
730 reaches that are most susceptible to geomorphic change. For susceptible reaches, a sediment  
731 budgeting approach (Frings et al., 2018) could be applied to quantify channel change using



732 repeat topographic surveys. These data could then be used to improve flood risk modelling,  
733 including the application of morphodynamic models (Williams et al., 2016).

734

735 Responses to river bank erosion by river managers range from hard engineering to prevent  
736 lateral erosion (Przedwojski et al., 2005) to the creation of erodible river corridors where rivers  
737 are given space to naturally migrate (Piégay et al., 2005; Biron et al., 2014). Within the  
738 Cagayan catchment, hard bank protection structures have been, and continue to be,  
739 constructed along eroding banks that are adjacent to vulnerable property, particularly  
740 residential areas. In temperate regions where rivers are subject to high rates of sediment  
741 supply, hard bank protection structures that narrow river corridors can cause increased  
742 aggradation (Davies et al., 2003; Siviglia et al., 2008) and thus can increase flood risk due to  
743 reduced channel capacity and greater risk of flood defence breaches. However, rivers that are  
744 confined by bank protection and subject to high rates of sediment supply may also respond  
745 by steepening and/or fining their bed to enable greater sediment transport rates (Eaton and  
746 Church, 2009; Madej et al., 2009). The complexity of these geomorphological responses to  
747 river corridor confinement and intermittent sediment supply suggests that further observational  
748 data and numerical scenario modelling is needed to enable a sustainable approach to  
749 managing river dynamism and land development within the Cagayan catchment.

750

## 751 5. Conclusions

752

753 Rates and patterns of channel and confluence migration, combined with channel pattern, width  
754 and sediment grain size analysis along ~85 km of the Cagayan River and a number of its  
755 tributaries suggest that sediment transport and deposition are key components of tropical river  
756 morphodynamics. In these fluvial systems, sediment loads are typically high and annual flow  
757 hydrographs are dominated by typhoon storms which generate several geomorphically  
758 effective flows each year. Typhoon related discharges mobilise and recycle large quantities of  
759 hillslope and floodplain sediment, which has a direct impact on channel morphology (channel

760 sinuosity, width, braiding intensity) and lateral channel and confluence migration rates. There  
761 is no clear evidence that land use change within the Cagayan catchment has led to an increase  
762 in lateral channel migration rates over the last ~40 years. In the case of the Cagayan River,  
763 spatial variations in floodplain width and heterogeneity may also enhance local rates of bed  
764 aggradation and channel mobility, most notably around major channel confluences where  
765 tributaries have larger or coarser sediment loads. An analysis of existing migration rate data  
766 in combination with new rates from the Cagayan River also suggest that channel migration  
767 rates are typically greater in tropical rivers than in temperate systems. Regions of increased  
768 bed aggradation at confluences and upstream of topographic valley constrictions may also  
769 explain why published relationships between slope and dimensionless discharge for  
770 discriminating braided and single-thread channels may not be fully appropriate for aggrading  
771 tropical river systems. We propose that these factors need to be taken into consideration in  
772 wider river and flood management programmes in these types of settings where flood risk  
773 mapping may need to incorporate channel dynamism and hard bank protection may result in  
774 geomorphological feedbacks that have adverse consequences for flood risk.

775

#### 776 Acknowledgements

777

778 This research was funded by the Scottish Funding Council, grant number SFC-AN-12-2017.  
779 We thank the City Government of Ilagan for supporting fieldwork access and logistics. Meghan  
780 Oliver provided the data for Fig. 9. We also thank Avijit Gupta and an anonymous reviewer for  
781 comments and discussions that have helped to improve this paper.

782

#### 783 Data availability

784

785 Satellite data used in the migration analysis was freely downloaded from the USGS Earth  
786 Explorer website (<http://earthexplorer.usgs.gov/>). IfSAR data were generated by Intermap Inc.  
787 for the National Mapping and Resource Information Authority (NAMRIA) between January and

788 July 2013. Digitised channel banks and centrelines are provided as ESRI Shapefiles in the  
789 online Supplementary Material, in addition to sinuosity and braiding data and sediment grain  
790 size statistics. The swath profiling tool from Clubb et al. (2017) is freely available to download  
791 from [http://github.com/LSDtopotools/LSDTopoTools\\_FloodplainTerraceExtraction](http://github.com/LSDtopotools/LSDTopoTools_FloodplainTerraceExtraction).  
792 Hydrological data were provided by the Bureau of Research Standards under the Philippines  
793 Department of Public Works and Highways. The dataset generated for this manuscript is  
794 available from the Mendeley data repository: DOI:10.17632/sn9mzzpxtn.2.

795

## 796 References

797

798 Aalto, R., Lauer, J.W., Dietrich, W.E., 2008. Spatial and temporal dynamics of sediment  
799 accumulation and exchange along Strickland River floodplains (Papua New Guinea)  
800 over decadal-to-centennial timescales. *Journal of Geophysical Research: Earth*  
801 *Surface* 113 (F01S04).

802 Alfieri, L., Bisselink, B., Dottori, F., Naumann, G., de Roo, A., Salamon, P., Wyser, K., Feyen,  
803 L., 2017. Global projections of river flood risk in a warmer world. *Earth's Future* 5 (2),  
804 171-182.

805 Ashmore, P. E., 2013. Morphology and Dynamics of Braided Rivers. In: Shroder, J. (Editor in  
806 Chief), Wohl, E. (Ed.), *Treatise on Geomorphology*. Academic Press, San Diego, CA,  
807 vol. 9, *Fluvial Geomorphology*, 289-312.

808 Ashworth, P.J., Lewin, J., 2012. How do big rivers come to be different? *Earth-Science*  
809 *Reviews*, 114 (1-2), pp.84-107.

810 Balderama, O. F. Alejo, L. A., Tongson, E., Rhia, E., Pantola, T., 2017. Development and  
811 Application of Corn Model for Climate Change Impact Assessment and Decision Support  
812 System: Enabling Philippine Farmers Adapt to Climate Variability In: Walter Leal Filho  
813 (Eds.), *Climate Change Research at Universities*, 373-387.

814 Best, J.L., Ashworth, P.J., 1997. Scour in large braided rivers and the recognition of sequence  
815 stratigraphic boundaries. *Nature* 387 (6630), 275-277.

816 Biron, P. M., Buffin-Bélanger, T., Larocque, M., Choné, G., Cloutier, C. A., Ouellet, M. A.,  
817 Demers, S., Olsen, T., Desjarlais, C., Eyquem, J., 2014. Freedom Space for Rivers: A  
818 Sustainable Management Approach to Enhance River Resilience, *Environmental*  
819 *Management* 54 (5), 1056-1073.

820 Church, M., 1992. Channel morphology and typology. *The Rivers Handbook: Hydrological and*  
821 *Ecological Principles*. P. Calow and G. Petts (editors). Blackwell Scientific Publications,  
822 Oxford, UK.

823 Church, M., 2006. Bed material transport and the morphology of alluvial river channels. *Ann.*  
824 *Rev. Earth Planet. Sci.* 34, 325-354.

825 Clubb, F.J., Mudd, S.M., Attal, M., Milodowski, D.T., Grieve, S.W., 2016. The relationship  
826 between drainage density, erosion rate, and hilltop curvature: Implications for sediment  
827 transport processes. *Journal of Geophysical Research: Earth Surface* 121 (10), 1724-  
828 1745.

829 Clubb, F.J., Mudd, S.M., Milodowski, D.T., Valters, D.A., Slater, L.J., Hurst, M.D., Limaye,  
830 A.B., 2017. Geomorphometric delineation of floodplains and terraces from objectively  
831 defined topographic thresholds. *Earth Surface Dynamics* 5 (3), 369-385.

832 Constantine, C.R., Dunne, T., Hanson, G.J., 2009. Examining the physical meaning of the  
833 bank erosion coefficient used in meander migration modeling. *Geomorphology* 106 (3-  
834 4), 242-252.

835 Constantine, J.A., Dunne, T., Ahmed, J., Legleiter, C., Lazarus, E.D., 2014. Sediment supply  
836 as a driver of river meandering and floodplain evolution in the Amazon Basin. *Nature*  
837 *Geoscience* 7 (12), 899-903.

838 Dade, W.B., 2000. Grain size, sediment transport and alluvial channel  
839 pattern. *Geomorphology* 35 (1-2), 119-126.

840 Darby, S.E., Leyland, J., Kumm, M., Räsänen, T.A., Lauri, H., 2013. Decoding the drivers of  
841 bank erosion on the Mekong river: The roles of the Asian monsoon, tropical storms, and  
842 snowmelt. *Water Resources Research* 49 (4), 2146-2163.

843 Davies, T.R., McSaveney, M.J., Clarkson, P.J. 2003. Anthropogenic aggradation of the Waiho  
844 River, Westland, New Zealand: microscale modelling. *Earth Surface Processes and*  
845 *Landforms* 28 (2), 209-218.

846 Dewan, A., Corner, R., Saleem, A., Rahman, M.M., Haider, M.R., Rahman, M.M., Sarker,  
847 M.H., 2017. Assessing channel changes of the Ganges-Padma River system in  
848 Bangladesh using Landsat and hydrological data. *Geomorphology* 276, 257-279.

849 Dietrich, W.E., Smith, J.D., Dunne, T., 1979. Flow and sediment transport in a sand bedded  
850 meander. *The Journal of Geology* 87 (3), 305-315.

851 Dingle, E.H., Sinclair, H.D., Attal, M., Milodowski, D.T., Singh, V., 2016. Subsidence control  
852 on river morphology and grain size in the Ganga Plain. *American Journal of Science* 316  
853 (8), 778-812.

854 Dixon, S.J., Smith, G.H.S., Best, J.L., Nicholas, A.P., Bull, J.M., Vardy, M.E., Sarker, M.H.,  
855 Goodbred, S., 2018. The planform mobility of river channel confluences: Insights from  
856 analysis of remotely sensed imagery. *Earth-Science Reviews* 176, 1-18.

857 Dunne, K.B., Jerolmack, D.J., 2018. Evidence of, and a proposed explanation for, bimodal  
858 transport states in alluvial rivers. *Earth Surface Dynamics* 6 (3), 583-594.

859 Durkee, E.F., Pederson, S.L., 1961. Geology of northern Luzon, Philippines. *AAPG Bulletin* 45  
860 (2), 137-168.

861 Eaton, B.C., Church, M., 2009. Channel stability in bed load-dominated streams with  
862 nonerodible banks: Inferences from experiments in a sinuous flume. *Journal of*  
863 *Geophysical Research: Earth Surface* 114 (F01024).

864 Eaton, B.C., Millar, R.G., Davidson, S., 2010. Channel patterns: Braided, anabranching, and  
865 single-thread. *Geomorphology* 120 (3-4), 353-364.

866 Ferguson, R.I., Cudden, J.R., Hoey, T.B., Rice, S.P., 2006. River system discontinuities due  
867 to lateral inputs: generic styles and controls. *Earth Surface Processes and Landforms*  
868 31, 1149–1166.

869 Ferguson, R., Hoey, T., 2008. Effects of tributaries on main-channel geomorphology. *River*  
870 *confluences, tributaries and the fluvial network*, 183-208.

871 Floresca, J.P., Paringit, E. C., 2017. Overview of the Program and the Pinacanauan de Ilagan  
872 River. In Paringit, E.C. (Ed.), LIDAR Surveys and Flood Hazard Mapping of the  
873 Philippines, University of the Philippines Training Center for Applied Geodesy and  
874 Photogrammetry, Quezon City, 371.

875 Forest Management Bureau, 2013. Philippine Forest Facts and Figures. Department of  
876 Environment and Natural Resources, Philippines. Second Edition.  
877 [[http://forestry.denr.gov.ph/pdf/ref/PF3\\_2013.pdf](http://forestry.denr.gov.ph/pdf/ref/PF3_2013.pdf); accessed online 04/09/2018]

878 Frings, R. M., Ten Brinke, W. B. M., 2018. Ten reasons to set up sediment budgets for river  
879 management, *International Journal of River Basin Management* 16 (1), 35-40.

880 Gabet, E.J., Mudd, S.M., 2010. Bedrock erosion by root fracture and tree throw: A coupled  
881 biogeomorphic model to explore the humped soil production function and the  
882 persistence of hillslope soils. *Journal of Geophysical Research: Earth Surface* 115 (F4).

883 Gran, K.B., Montgomery, D.R., Halbur, J.C., 2011. Long-term elevated post-eruption  
884 sedimentation at Mount Pinatubo, Philippines. *Geology* 39 (4), 367-370.

885 Hergarten, S., Robl, J., Stüwe, K., 2014. Extracting topographic swath profiles across curved  
886 geomorphic features. *Earth Surface Dynamics* 2 (1), 97-104.

887 Hickin, E.J., Nanson, G.C., 1975. The character of channel migration on the Beaton River,  
888 northeast British Columbia, Canada. *Geological Society of America Bulletin* 86 (4), 487-  
889 494.

890 Hilton, R.G., Galy, A., Hovius, N., Chen, M.C., Horng, M.J., Chen, H., 2008. Tropical-cyclone-  
891 driven erosion of the terrestrial biosphere from mountains. *Nature Geoscience* 1 (11),  
892 759-762.

893 Hooke, J.M., 2007. Spatial variability, mechanisms and propagation of change in an active  
894 meandering river. *Geomorphology* 84 (3-4), 277-296.

895 Hooke, J.M., 1980. Magnitude and distribution of rates of river bank erosion. *Earth Surface*  
896 *Processes* 5 (2), 143-157.

897 Horton, A.J., Constantine, J.A., Hales, T.C., Goossens, B., Bruford, M.W., Lazarus, E.D.,  
898 2017. Modification of river meandering by tropical deforestation. *Geology* 45 (6), 511-  
899 514.

900 Hudson, P.F., Kesel, R.H., 2000. Channel migration and meander-bend curvature in the lower  
901 Mississippi River prior to major human modification. *Geology* 28 (6), 531-534.

902 Lagmay, A. M. F., Racoma, B.A., Aracan, K.A., Alconis-Ayco, J., Saddi, I.L., 2017.  
903 Disseminating near-real-time hazards information and flood maps in the Philippines  
904 through Web-GIS, *Journal of Environmental Sciences* 59, 13-23.

905 Lane, S. N., Tayefi, V., Reid, S.C., Yu, D., Hardy, R.J., 2007. Interactions between sediment  
906 delivery, channel change, climate change and flood risk in a temperate upland  
907 environment, *Earth Surface Processes and Landforms* 32 (3), 429-446.

908 Latrubesse, E.M., Stevaux, J.C., Sinha, R., 2005. Tropical rivers. *Geomorphology* 70 (3), 187-  
909 206.

910 Lauer, J.W., Parker, G., 2008. Net local removal of floodplain sediment by river meander  
911 migration. *Geomorphology* 96 (1-2), 123-149.

912 Lawler, D.M., 1993. The measurement of river bank erosion and lateral channel change: a  
913 review. *Earth Surface Processes and Landforms* 18 (9), 777-821.

914 Leopold, L.B., Maddock, T., 1953. The hydraulic geometry of stream channels and some  
915 physiographic implications (Vol. 252). US Government Printing Office.

916 Leopold, L.B., Wolman, M.G., 1957. River channel patterns: braided, meandering, and  
917 straight. US Geological Survey Professional Paper 282-B, 85.

918 Madej M.A., Sutherland D.G., Lisle T.E., Pryor, B. 2009. Channel responses to varying  
919 sediment input: A flume experiment modeled after Redwood Creek, California.  
920 *Geomorphology* 103, 507–519.

921 McMillan, H., Freer, J., Pappenberger, F., Krueger, T., Clark, M., 2010. Impacts of uncertain  
922 river flow data on rainfall- runoff model calibration and discharge  
923 predictions. *Hydrological Processes* 24 (10), 1270-1284.

924 Micheli, E.R., Kirchner, J.W., Larsen, E.W., 2004. Quantifying the effect of riparian forest  
925 versus agricultural vegetation on river meander migration rates, Central Sacramento  
926 River, California, USA. *River Research and Applications* 20 (5), 537-548.

927 Milliman, J.D., Meade, R.H., 1983. World-wide delivery of river sediment to the oceans. *The*  
928 *Journal of Geology* 91 (1), 1-21.

929 Miller, D.J., Benda, L.E., 2000. Effects of punctuated sediment supply on valley-floor  
930 landforms and sediment transport. *Geological Society of America Bulletin* 112 (12),  
931 1814-1824.

932 Mines and Geosciences Bureau. 2010. *Geology of the Philippines, Second Edition*. Pp. 115-  
933 116, 120-121.

934 Montgomery, D.R., Brandon, M.T., 2002. Topographic controls on erosion rates in tectonically  
935 active mountain ranges. *Earth and Planetary Science Letters* 201 (3-4), 481-489.

936 Mosley, M.P., 1981. Semi-determinate hydraulic geometry of river channels, South Island,  
937 New Zealand. *Earth Surface Processes and Landforms* 6 (2), 127-137.

938 Mueller, E.R., Pitlick, J., 2014. Sediment supply and channel morphology in mountain river  
939 systems: 2. Single thread to braided transitions. *Journal of Geophysical Research: Earth*  
940 *Surface* 119 (7), 1516-1541.

941 Parker G., 1979. Hydraulic geometry of active gravel rivers. *Journal of the Hydraulics Division*  
942 *ASCE* 105, 1185–1201.

943 Perron, J.T., Dietrich, W.E., Kirchner, J.W., 2008. Controls on the spacing of first-order  
944 valleys. *Journal of Geophysical Research: Earth Surface* 113 (F04016).

945 Piégay, H., Darby, S.E., Mosselman, E., Surian, N., 2005. A review of techniques available for  
946 delimiting the erodible river corridor: a sustainable approach to managing bank erosion,  
947 *River Research and Applications* 21 (7), 773-789.

948 Plink-Björklund, P., 2015. Morphodynamics of rivers strongly affected by monsoon  
949 precipitation: review of depositional style and forcing factors, *Sedimentary Geology* 323,  
950 110-147.



951 Principe, J.A., 2012. Exploring climate change effects on watershed sediment yield and land  
952 cover-based mitigation measures using swat model, RS and GIS: case of Cagayan  
953 River Basin, Philippines. *Int. Arch. Photogram. Rem. Sens. Spatial Inform. Sci.* 39, 193-  
954 198.

955 Przedwojski, B., Błażejowski, R., Pilarczyk, K. W. 1995. River training techniques:  
956 fundamentals, design and applications. AA Balkema, Rotterdam, 625.

957 Rice, S., Church, M., 1996. Sampling surficial fluvial gravels: The precision of size distribution  
958 percentile estimates. *Journal of Sedimentary Research* 66, 654-65.

959 Richards, K.S., 1980. A note on changes in channel geometry at tributary junctions. *Water*  
960 *Resources Research* 16 (1), 241-244.

961 Rojas, D.S., 2014. Abuan Integrated Watershed Program: Flood Hydrology and Hydraulics.  
962 WWF-Philippines.

963 Samuels, P.G., 1989. Backwater lengths in rivers. *Proceedings of the Institution of Civil*  
964 *Engineers* 87 (4), 571-582.

965 Scatena, F.N., Gupta, A., 2013. Streams of the montane humid tropics. In: Shroder, J. (Editor  
966 in Chief), Wohl, E. (Ed.), *Treatise on Geomorphology*. Academic Press, San Diego, CA,  
967 vol. 9, *Fluvial Geomorphology*, 595–611.

968 Schumm, S.A., 1985. Patterns of alluvial rivers. *Annual Review of Earth and Planetary*  
969 *Sciences* 13 (1), 5-27.

970 Siviglia A., Repetto R., Zolezzi G., Tubino, M., 2008. River bed evolution due to channel  
971 expansion: general behaviour and application to a case study (Kugart River, Kyrgyz  
972 Republic). *River Research and Applications* 24, 1271–1287.

973 Slater, L. J., 2016. To what extent have changes in channel capacity contributed to flood  
974 hazard trends in England and Wales?, *Earth Surface Processes and Landforms* 41 (8),  
975 1115-1128.

976 Smith, N.D., Smith, D.G., 1984. William River: An outstanding example of channel widening  
977 and braiding caused by bed-load addition. *Geology* 12, 78–82.

978 Suizu, T.M., Nanson, G.C., 2018. Temporal and spatial adjustments of channel migration and  
979 planform geometry: responses to ENSO driven climate anomalies on the tropical freely-  
980 meandering Aguapeí River, São Paulo, Brazil. *Earth Surface Processes and Landforms*  
981 43, 1636-1647.

982 Syvitski, J.P., Cohen, S., Kettner, A.J., Brakenridge, G.R., 2014. How important and different  
983 are tropical rivers? An overview. *Geomorphology* 227, 5-17.

984 Tolentino, P.L.M., Poortinga, A., Kanamaru, H., Keesstra, S., Maroulis, J., David, C.P.C.,  
985 Ritsema, C.J., 2016. Projected impact of climate change on hydrological regimes in the  
986 Philippines. *PloS one* 11 (10), 1-14.

987 Tucker, G.E., Slingerland, R., 1997. Drainage basin responses to climate change. *Water*  
988 *Resources Research* 33 (8), 2031-2047.

989 Van den Berg, J.H., 1995. Prediction of alluvial channel pattern of perennial  
990 rivers. *Geomorphology* 12 (4), 259-279.

991 Van der Ploeg, J., Van Weerd, M., Masipiqueña, A.B., Persoon, G.A., 2011. Illegal logging in  
992 the Northern Sierra Madre Natural Park, the Philippines. *Conservation and Society* 9 (3),  
993 202-215.

994 Williams, R.D., Measures, R., Hicks, D.M., Brasington, J., 2016. Assessment of a numerical  
995 model to reproduce event-scale erosion and deposition distributions in a braided  
996 river. *Water Resources Research* 52 (8), 6621-6642.

997 Wobus, C.W., Tucker, G.E., Anderson, R.S., 2006. Self-formed bedrock  
998 channels. *Geophysical Research Letters* 33 (18).

999 Wolman, M.G., 1954. A method of sampling coarse river-bed material. *EOS, Transactions*  
1000 *American Geophysical Union* 35 (6), 951-956.

1001 Wolman, M.G., Leopold, L.B., 1957. River flood plains: some observations on their  
1002 formation (No. 282-C). US Government Printing Office, 87-109.

1003

1004

1005

1006 Supplementary Material

1007

1008 Table S1. Satellite imagery sources and horizontal spatial resolution used in this study.

<b>Year (Month)</b>	<b>Dataset</b>	<b>Horizontal spatial resolution (m)</b>
1973 (June)	Landsat 1 MSS	60
1990 (Feb)	Thematic Mapper 1984-1997	30-50
2001 (June)	ETM+ Pan sharpened mosaic	14.25
2008 (June)	Landsat 5 TM	30
2017 (April/Nov)	Sentinel 2	10-20 (depending on band combination used)
2017 (July)	RapidEye	5

1009

1010